Feng, S., Vardanega, P., Ibraim, E., Widyatmoko, I., & Ojum, C. (2019). Permeability assessment of some granular mixtures. *Géotechnique*, *69*(7), 646–654. https://doi.org/10.1680/jgeot.17.t.039, https://doi.org/10.1680/jgeot.17.T.039

TECHNICAL NOTE

Permeability assessment of some granular mixtures

S. FENG*, P. J. VARDANEGA†, E. IBRAIM‡, I. WIDYATMOKO§ and C. OJUM‖

This note presents some constant-head permeability test results on 30 granular mixtures. These data are then interpreted using the grading entropy approach, as well as the 'Hazen', 'Shepherd', 'Kozeny–Carman' and 'Chapuis' models. The predictive power of each of the five methods is compared. A correlation between the normalised grading entropy coordinates and the coefficient of permeability is presented. Permeability zones on the normalised entropy diagram are identified.

KEYWORDS: filters; permeability; statistical analysis

INTRODUCTION

Permeability is a key factor to consider when assessing the durability and service quality of road pavement structures (e.g. Thom, 2014). This note presents some results of constant-head permeability testing on 30 aggregate mixtures. These results are used to compare five models namely 'Hazen' (Hazen, 1893, 1895, 1911), 'Shepherd' (Shepherd, 1989), 'Kozeny–Carman' (Kozeny, 1927; Carman, 1937, 1939), 'Chapuis' (Chapuis, 2004, 2012) and an approach which uses the grading entropy co-ordinates (see Lőrincz *et al.* (2005)) as predictors of hydraulic conductivity, hereafter referred to as the 'grading entropy' model.

TRADITIONAL MODELS FOR PERMEABILITY

Permeability K (L^2) is often described in terms of the coefficient of permeability, k (L/T), which depends on both the intrinsic properties of the porous medium and the pore fluid; equation (1) (e.g. Chapuis & Aubertin, 2003)

$$k = \frac{\gamma_w}{\mu_w} K \tag{1}$$

where γ_w is the unit weight of the permeant and μ_w is the dynamic viscosity of the permeant.

The coefficient of permeability is related to the effective particle size. Hazen's formulation (Hazen, 1893, 1895, 1911) can be expressed as follows

$$k = (0{\cdot}7 + 0{\cdot}03t) C_H D_{10}^2 \tag{2}$$

where t is the temperature (°C); D_{10} (L) is the sieve size (aperture) through which 10% of the material would pass; and C_H (L^{-1}/T) is the Hazen empirical coefficient. According to the work of Hazen (1893, 1895) C_H is approximately 1000 μm^{-1}/d, subsequently, he suggested a range of values from 400 to 1200 (Hazen, 1911).

Shepherd (1989) presented a revised version of Hazen's formulation with a revised exponent on D_{10}

$$K = cD_{10}^x \tag{3}$$

where c is a dimensionless constant and x generally varies from 1·65 to 1·85 (it is noted that Shepherd did not specify the representative particle size; in this note, however, D_{10} is used).

The Kozeny–Carman equation (Kozeny, 1927; Carman, 1937, 1939) is another approach to estimate the coefficient of permeability (form shown as in Carrier (2003))

$$k = \left(\frac{\gamma}{\mu}\right)\left(\frac{1}{C_{K\text{-}C}}\right)\left(\frac{1}{S_A^2}\right)\left(\frac{e^3}{1+e}\right) \tag{4}$$

where γ is the unit weight of the permeant; μ is its viscosity; S_A is the specific surface area per unit volume of particles; e is the void ratio; and $C_{K\text{-}C}$ is the Kozeny–Carman coefficient, which accounts for the tortuosity and shape of the particles. According to Carman (1939), $C_{K\text{-}C}$ can be found experimentally to be approximately 5 for uniform spheres. Ozgumus *et al.* (2014) presented a detailed review of published $C_{K\text{-}C}$ values, within which the lowest $C_{K\text{-}C}$ value is 3·4 measured in peat beds (Mathavan & Viraraghavan, 1992) and the highest is experimentally found to be 12·81 in fibrous and granular beds (Li & Gu, 2005). Another commonly used form of the equation is given by Chapuis & Aubertin (2003)

$$k = C\frac{\boldsymbol{g}}{\mu_w \rho_w}\frac{e^3}{S_s^2 D_R^2 (1+e)} \tag{5}$$

where $C = 1/C_{K-C}$; $\boldsymbol{g}$ is gravitational acceleration; ρ_w is the density of the permeant; D_R is the specific gravity of solid ($D_R = \rho_s/\rho_w$, ρ_s is the density of solid); and S_s is the specific surface of the solid. Chapuis & Légaré (1992) proposed a method to estimate S_s of the soil based on simple geometric considerations, which is

$$S_s = \frac{6}{\rho_s}\sum\left(\frac{P_{No\,D} - P_{No\,d}}{d}\right) \tag{6}$$

Manuscript received 17 August 2017; revised manuscript accepted 12 July 2018.
Discussion on this paper is welcomed by the editor.

* Department of Civil Engineering, University of Bristol, Bristol, UK) (Orcid:0000-0002-3837-6762).
† Department of Civil Engineering, University of Bristol, Bristol, UK (Orcid:0000-0001-7177-7851).
‡ Department of Civil Engineering, University of Bristol, Bristol, UK.
§ Pavement Engineering, Centre of Excellence for Asset Consultancy, AECOM, Nottingham, UK (Orcid:0000-0003-1252-3979).
‖ Pavement Engineering, Centre of Excellence for Asset Consultancy, AECOM, Nottingham, UK.

Table 1. Applications of grading entropy theory

Research field	Publication
Dry density of granular soil	Lőrincz (1990), Lőrincz *et al.* (2008) and Imre *et al.* (2009)
Characterisation of sand mixture	Imre *et al.* (2008) and Imre *et al.* (2015)
Particle loss	McDougall *et al.* (2013a) and McDougall *et al.* (2013b)
Soil crushing, particle size evolution/degradation	Lőrincz *et al.* (2005), Imre *et al.* (2012), Lőrincz *et al.* (2015b) and Imre & Fityus (2018)
Piping	Imre *et al.* (2012) and Imre *et al.* (2015)
Dispersion	Imre *et al.* (2012)
Structural stability of filters	Imre *et al.* (2012) and Lőrincz *et al.* (2015a)
Permeability of asphalt concrete	James (2015), Feng (2017) and Feng *et al.* (2018)

where $(P_{\mathrm{No}\,D} - P_{\mathrm{No}\,d})$ is the percentage by weight of particles between size D (the larger one) and size d (the smaller one). In this technical note 0·0375 mm is adopted as the smaller particle size, as the smallest available sieve was 0·075 mm, and the grading entropy calculation requires a series of successively doubled sieve sizes.

Chapuis (2004) developed a predictive equation that includes the term $e^3/(1+e)$ in the Kozeny–Carman equation and D_{10}^2 in Hazen's formulation; the proposed power-law relationship between k and $D_{10}^2 e^3/(1+e)$ based on a regression analysis is given as

$$k\ (\mathrm{cm/s}) = 2{\cdot}4622\left[D_{10}^2 e^3/(1+e)\right]^{0{\cdot}7825} \tag{7}$$

where D_{10} is in millimetres. According to Chapuis (2012), equation (7) can be used for non-plastic materials, but may not be accurate enough when applied to crushed materials.

GRADING ENTROPY FRAMEWORK

The grading entropy theory is comprehensively reviewed in Singh (2014) and has also been used in several publications listed in Table 1 to study various geotechnical phenomena.

The grading entropy framework considers, according to Imre *et al.* (2012), 'the distribution of particle sizes in a soil is a reflection of its order or disorder of nature'. It is attributed to Lőrincz's 1986 doctoral thesis (Lőrincz *et al.*, 2005; Singh, 2014) by applying entropy theory (Shannon, 1948) to the particle size distribution (PSD), thereby establishing a vectorial depiction of gradation variation (McDougall *et al.*, 2013b). The following explanation of the theory is largely based on that presented in Singh (2014), whose notation is used unless otherwise stated.

Shannon (1948) defined the entropy $H(x)$ as

$$H(x) = -\sum p_i \log p_i \tag{8}$$

where p_i is the probability of a system being in cell i. While in grading entropy theory a double statistical cell system (see Fig. 1) – which consists of a fraction grid (i) (primary cell system) successively doubled in width and a secondary cell system (j) with a uniform width d_0 – to subdivide the fraction cells in the fraction grid, is introduced in this theory. The number of secondary cells in a fraction i is

$$C_i = \frac{d_{i+1} - d_i}{d_0} \tag{9}$$

where d_i is the width of the fraction i. The relative frequency x_i can be obtained using

$$x_i = \frac{M_i}{M} \tag{10}$$

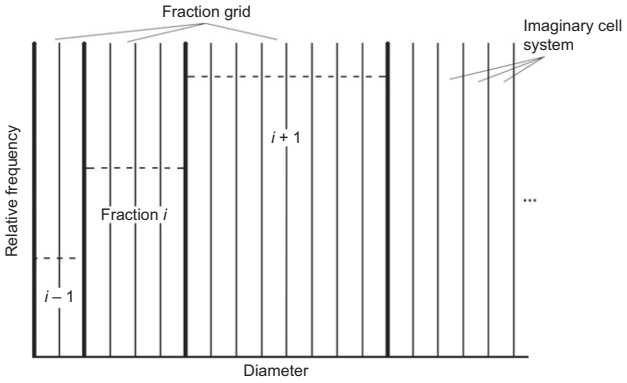

Fig. 1. Relationship between fraction and elementary cell grid (after Lőrincz *et al.* (2005), used with permission from ASCE)

where M_i is the weight of particles in fraction i (which is equivalent to the percentage of particles retained on the sieve) and M is the total weight of the sample mixture. Thus the relative frequency of the jth secondary cell in the ith fraction is

$$p_{ij} = \frac{x_i}{C_i} \tag{11}$$

By substituting the relative frequency p_{ij} into equation (8), the ultimate form of grading entropy, S, of an arbitrary mixture could be computed as follows (see Lőrincz (1990) for a full derivation)

$$S = -\sum_{i=1}^{N} x_i \log_2 x_i + \sum_{i=1}^{N} x_i \log_2 C_i \tag{12}$$

where x_i is the relative frequency of fraction i and N is the number of fractions. As the grading entropy equation consists of two parts, which respectively relate to the elementary cell system C_i and the real fractions x_i, the grading entropy is split into two coordinates, namely base entropy S_0 and the entropy increment ΔS

$$S_0 = \sum_{i=1}^{N} x_i \log_2 C_i \tag{13}$$

$$\Delta S = -\sum_{i=1}^{N} x_i \log_2 x_i \tag{14}$$

Logarithm base 2 is chosen to yield a simple form of eigen-entropy S_{0i} (Singh, 2014)

$$S_{0i} = \log_2 2^{i-1} = i - 1 \tag{15}$$

By making the base entropy S_0 constrained to a fixed interval for a different number of fractions, and the

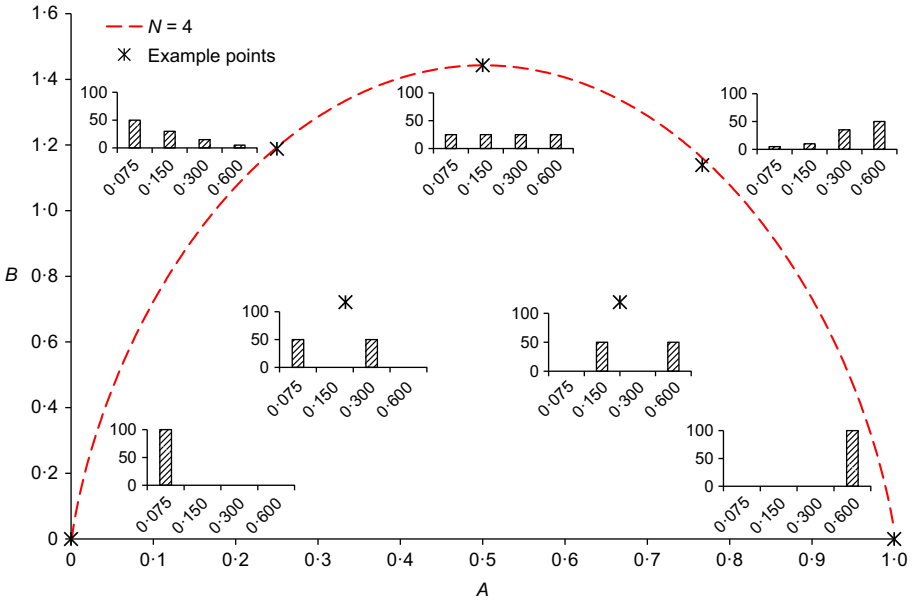

Fig. 2. Effect of gradation changes on the *A* and *B* parameters (based on McDougall *et al.* (2013a, 2013b))

entropy increment ΔS independent with N, two normalised entropy coordinates A (the relative base grading entropy) and B (normalised entropy increment) are obtained (see the online supplementary material for a full calculation example)

$$A = \frac{S_0 - S_{\min}}{S_{0\max} - S_{0\min}} = \frac{\sum_{i=1}^{N} x_i(i-1)}{N-1} \tag{16}$$

$$B = -\frac{\sum_{i=1}^{N} x_i \log_2 x_i}{\log N} \tag{17}$$

Based on the normalised entropy coordinates A and B, any grading curve can be interpreted and plotted as a single point on the normalised diagram. However, Imre *et al.* (2012) explained that, for an ongoing change in PSD (as a consequence of grain crushing, or soil erosion) or for materials with different PSDs, the variation in fraction number N can induce a discontinuity in the normalised entropy path. In order to remove this discontinuity, 'zero' fractions (coarser or finer fractions with zero particle frequency), which leave the non-normalised grading entropy unaffected, can be introduced in the analysis (see Imre *et al.* (2012)). The variations in gradation are depicted in a normalised entropy diagram to show the effect of changing PSD (see Fig. 2). McDougall *et al.* (2013b) explains that the relative base entropy A reflects the skewness (symmetry) of a gradation curve, while the normalised entropy increment B measures peakiness (kurtosis) of a distribution, as shown in Fig. 2. With the aid of the grading entropy diagram, variations in gradation can be recorded in one plot rather than a family of gradation curves, as schematically shown in Fig. 2.

Previously secondary cell widths d_0 were taken as 2^{-17} mm (e.g. Lőrincz, 1990) and 2^{-22} mm (e.g. Imre *et al.*, 2009). As previously stated in this analysis 0·0375 mm is used to enable the use of the grading entropy calculation. It should be noted that the tested mixtures did not have particle sizes less than this minimum value.

Based on the normalised grading entropy equations, for a certain fraction number N, the maximum normalised entropy increment (B) curve is fixed (see the calculation process in Singh (2014)); however, with different fraction numbers, N, the variation of the maximum increment curve is rather unnoticeable (cf. Imre *et al.*, 2008).

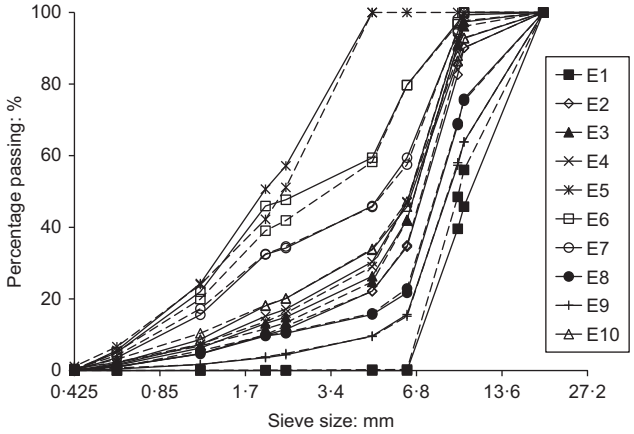

Fig. 3. PSDs of gradation type E examined before (solid lines) and after (dashed lines) permeability test

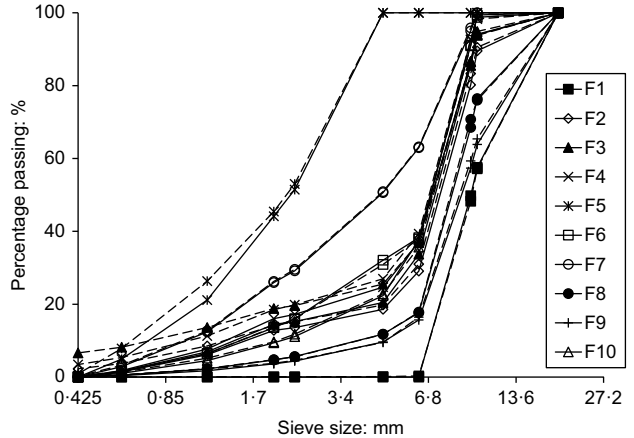

Fig. 4. PSDs of gradation type F examined before (solid lines) and after (dashed lines) permeability test

MATERIAL TESTING

The aggregates used in this study comprised a crushed basalt and a less rounded crushed gritstone. The nominal maximum aggregate size of the mixture is 10 mm. The aggregate abrasion value, Los Angeles abrasion, shape (flakiness index) and water absorption of the test material were 6, 10, 22 and 1·6%, respectively, which suggest the aggregates have high resistance to abrasion and relatively low water absorption. As for the flakiness index, in practice most designed asphalt mixtures specify a value of not greater than 25%; the lower the value, the more onerous the requirements.

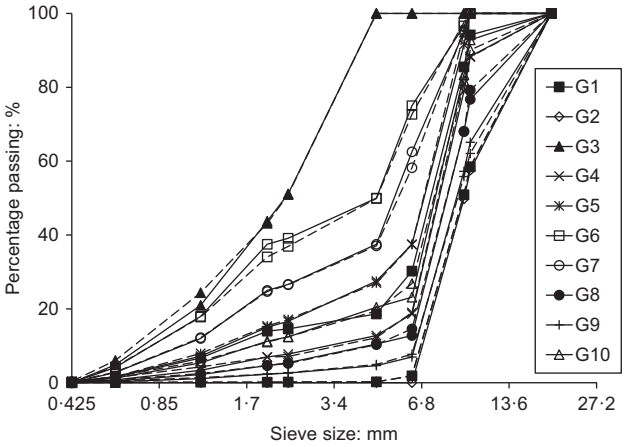

Fig. 5. PSDs of gradation type G examined before (solid lines) and after (dashed lines) permeability test

Three different PSDs (denoted as E, F, G) of the gravel component of pavement asphalt surfacing mixtures were used as a guide to develop a family of gradation curves employed for the permeability testing in this paper. Thirty different samples were fabricated, and the permeabilities were assessed using constant head testing. For each sample, the PSD was also re-examined (sieving test procedure generally followed ASTM (2014)) after the permeability test. Figures 3–5 present the PSDs before and after permeability test (before in solid lines, after in dashed lines). Some very minor variations of the PSDs before and after testing were noticed, most likely attributed to particle crushing or the flushing out of some fines during testing. Given these minor variations shown on Figs 3–5, the gradation parameters (D_{10}, D_{50}) used throughout the analysis are the averaged values from the before and after test PSDs, and the grading entropy parameters (A, B) are calculated based on the averaged PSDs.

The procedures adopted in the permeability testing generally followed BS 1377-5, chapter 5 (BSI, 1990). All the samples were compacted in four layers, and each layer was compacted manually by applying 70 blows using a sliding cylindrical tamper of 50 mm dia. and 2·5 kg self-weight.

Throughout the experimental programme, the total height of the samples was ≈320 mm, while an amount of 3·2 kg of material in the fully dried state was used. The dimensions of the samples (the permeameter had a diameter of 90 mm) and the dry weight of all 30 samples were measured and recorded. The temperature of the permeant (water) was monitored. All the permeability test results, including temperature test

Table 2. Summary of test results

Mixture sample	Measured k: mm/s	Water t: °C	$k_{20°C}$: mm/s*	Void ratio†	A	B	D_{10}: mm	D_{50}: mm	C_U	C_Z	Class‡
E1	476·61	17·8	505·20	0·85	0·94	0·46	7·02	9·93	1·66	0·88	GP
E2	80·38	17·9	86·81	0·68	0·84	0·78	2·01	7·29	3·96	2·05	GP
E3	56·71	15·8	62·95	0·71	0·83	0·76	1·66	6·82	4·50	2·15	GW
E4	49·89	15·8	55·38	0·68	0·81	0·80	1·49	6·51	4·84	2·13	GW
E5	5·44	17·8	5·76	0·61	0·64	0·80	0·72	2·17	3·68	1·01	GW
E6	7·76	17·9	8·15	0·62	0·72	1·01	0·78	3·24	6·22	0·62	GP
E7	9·81	18·5	10·31	0·56	0·76	0·95	0·88	5·26	7·29	0·62	GP
E8	89·25	17·7	94·61	0·70	0·87	0·78	2·12	8·21	4·19	2·47	GW
E9	164·39	17·8	174·25	0·75	0·91	0·69	4·86	8·92	1·99	1·16	GP
E10	25·51	17·3	27·55	0·62	0·81	0·92	1·22	6·58	6·02	1·85	GW
F1	501·07	15·4	561·20	0·84	0·94	0·46	6·94	9·56	1·52	0·93	GP
F2	28·77	19·8	28·77	0·59	0·84	0·78	1·54	7·54	5·31	3·17	GP
F3	16·27	19·9	16·27	0·53	0·82	0·83	1·15	7·22	6·82	3·50	GP
F4	19·95	20·1	19·95	0·56	0·81	0·77	1·23	6·99	6·15	2·97	GW
F5	3·78	15·8	4·19	0·51	0·65	0·80	0·72	2·25	3·81	1·02	GW
F6	14·11	17·9	14·81	0·61	0·82	0·82	1·58	7·02	4·81	1·69	GW
F7	43·61	18·3	45·79	0·67	0·76	0·96	1·02	4·66	5·77	0·98	GP
F8	123·78	17·9	129·97	0·79	0·89	0·70	4·07	8·29	2·19	1·37	GP
F9	163·74	17·7	173·57	0·75	0·91	0·69	4·85	8·87	1·98	1·16	GP
F10	55·74	17·3	60·20	0·71	0·84	0·76	2·09	7·16	3·74	1·91	GP
G1	52·33	15·7	58·61	0·66	0·84	0·73	1·54	7·46	5·24	3·23	GP
G2	277·87	16·5	302·88	0·75	0·94	0·46	6·89	9·48	1·51	0·93	GP
G3	7·07	16·5	7·71	0·54	0·65	0·77	0·75	2·31	3·72	1·02	GW
G4	145·03	19	149·38	0·73	0·87	0·66	3·58	7·93	2·36	1·57	GP
G5	45·25	17·7	47·97	0·66	0·82	0·76	1·44	7·02	5·26	2·44	GW
G6	8·68	17·5	9·29	0·60	0·74	0·95	0·84	4·75	6·40	0·66	GP
G7	14·47	17·4	15·49	0·58	0·78	0·86	1·05	5·60	5·98	1·48	GW
G8	200·78	17·5	214·83	0·74	0·89	0·68	4·57	8·44	1·98	1·28	GP
G9	276·14	17·4	295·46	0·74	0·92	0·60	6·47	9·07	1·51	0·96	GP
G10	56·46	17·9	60·98	0·67	0·85	0·77	1·83	7·69	4·50	2·86	GW

*$k_{20°C} = k_{measured}(v_{test\ t}/v_{20°C})$, where v is the kinematic viscosity.
†Void ratio is calculated according to $e = (V\rho/m) - 1$, where V is the total volume of the sample; ρ is the density of the solid particles (2720 kg/m^3 as measured in the laboratory); and m is the dry mass of the sample.
‡GW, well-graded gravel, $C_U > 4$ and $1 < C_Z < 3$ (Holtz *et al.*, 2011); GP, poorly graded gravel, $C_U < 4$ or $C_Z > 1$, $C_Z > 3$ (Holtz *et al.*, 2011).

condition, corrected permeability, sample void ratio (e) and other gradation parameters (D_{10}, D_{50}, C_U, C_Z) are summarised and listed in Table 2 (for further information on the testing see Feng (2017)).

ANALYSIS

The experimental results are now examined using the 'Hazen', 'Shepherd', 'Kozeny–Carman', 'Chapuis' and 'grading entropy' models.

Hazen's model

The temperature of the permeant (water) fluctuated between 15·4 and 20·1°C, so the measured k values were corrected to 20°C for the subsequent analysis and equation (2) becomes

$$k_{20°C} = 1{\cdot}3 C_H D_{10}^2 \tag{18}$$

Figure 6(a) shows the fitted relationship between $k_{20°C}$ and the D_{10}^2, which gives

$$k_{20°C} = 8{\cdot}98 D_{10}^2 \quad r = 0{\cdot}95,\ R^2 = 0{\cdot}90,\ n = 30,\ p < 0{\cdot}0001 \tag{19}$$

The C_H calculated is 6·91 mm^{-1}/s, which is in the range (1 to 1000 cm^{-1}/s) stated by Carrier (2003). The accompanying measured $k_{20°C}$ plotted against predicted $k_{20°C}$ (using equation (19)) is shown in Fig. 6(b). The predicted–measured plot (Fig. 6(b)) shows that 12 out of 30 data points lie outside the ±50% margins and 20% of data points fall beneath the line of equality (45° line), with 80% of the data points lying above the line of equality. For this dataset equation (19) tends to under-predict $k_{20°C}$.

Shepherd's model

Figure 7(a) gives the fitted line between $\ln k_{20°C}$ and $\ln D_{10}$, which is

$$\ln k_{20°C} = 1{\cdot}73 \ln D_{10} + 2{\cdot}76 \quad r = 0{\cdot}95,\ R^2 = 0{\cdot}90,\ n = 30,\ p < 0{\cdot}0001 \tag{20}$$

which can be rearranged to

$$k_{20°C} = 15{\cdot}8 D_{10}^{1{\cdot}73} \tag{21}$$

The exponent of 1·73 (in equation (21)) conforms with the findings of Shepherd (1989), who suggested a range of 1·65 to 1·85. The predicted plotted against measured plot (Fig. 7(b)) shows that nine out of 30 data points lie outside the ±50% margins and 50% of the data points fall above and below the line of equality. Therefore, for this dataset, equation (21) tends to predict $k_{20°C}$ generally to within ±50% while noting that the seven out of the nine data points outside this range represent under-predictions.

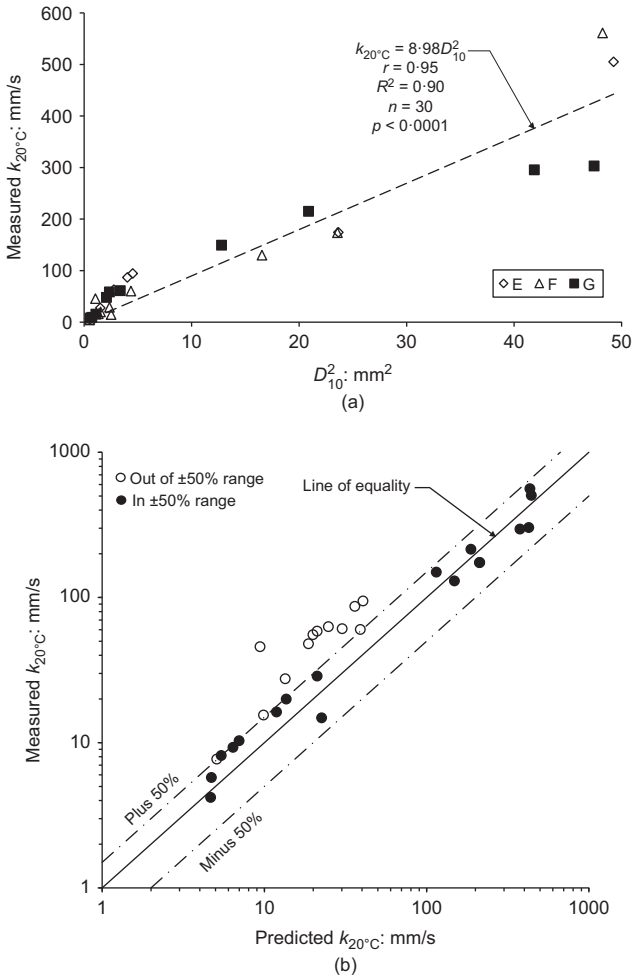

Fig. 6. (a) k plotted against D_{10}^2. (b) Predicted k compared to measured k (equation (19))

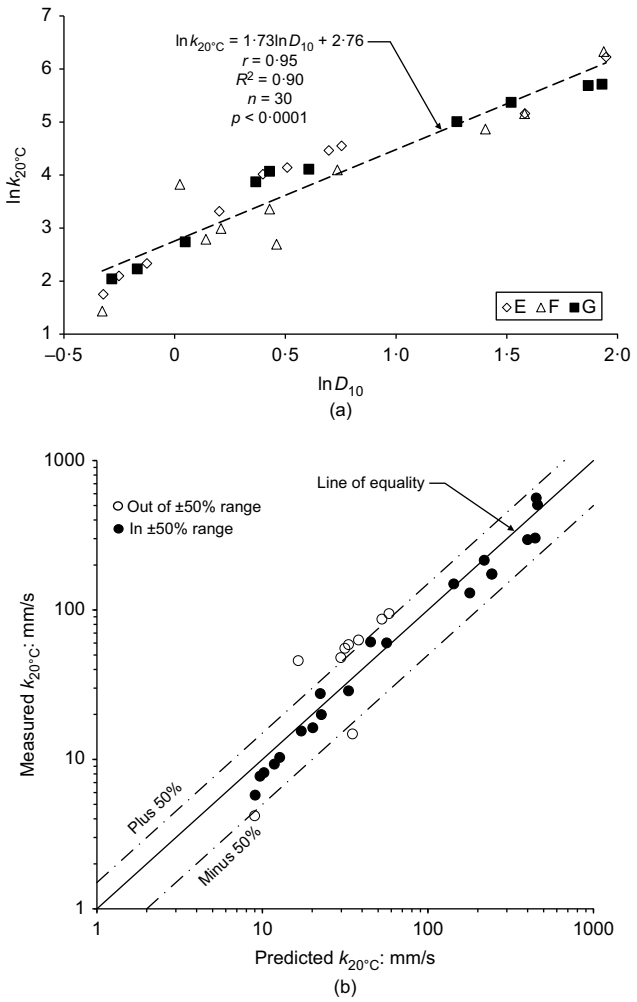

Fig. 7. (a) $\ln k$ plotted against $\ln D_{10}$. (b) Predicted k compared to measured k (equation (21))

Kozeny–Carman model

Figure 8(a) shows the relationship between $k_{20°C}$ and $(\boldsymbol{g}/\mu_w\rho_w)[e^3/S_s^2D_R^2(1+e)]$, which is

$$k_{20°C} = 0{\cdot}10\frac{\boldsymbol{g}}{\mu_w\rho_w}\frac{e^3}{S_s^2D_R^2(1+e)} \quad (22)$$
$$r = 0{\cdot}97,\ R^2 = 0{\cdot}94,\ n = 30,\ p < 0{\cdot}0001$$

For equation (22) the C calculated is 0·1, which corresponds to $C_{K\text{-}C}$ of 10 (see equation (4)). This value falls between the upper (12·81 for fibrous and granular beds) and lower (3·4 for peat beds) bounds given in the review by Ozgumus *et al.* (2014). The predicted plotted against measured plot (Fig. 8(b)), shows that seven out of 30 data points lie outside the ±50% margins and 16·7% of the data points fall beneath the line of equality, while the remainder of the data points lie above the line of equality. Therefore, for this dataset, equation (22) tends to yield slightly unsymmetrical (under) predictions of $k_{20°C}$.

Chapuis' model

Figure 9(a) presents the fitted correlation between $\ln k_{20°C}$ and $\ln[D_{10}^2e^3/(1+e)]$, which is

$$\ln k_{20°C} = 0{\cdot}73\ln\left(\frac{D_{10}^2e^3}{1+e}\right) + 4{\cdot}184 \quad (23)$$
$$r = 0{\cdot}95,\ R^2 = 0{\cdot}91,\ n = 30,\ p < 0{\cdot}0001$$

which can be rearranged to

$$k_{20°C} = 65{\cdot}6\left(\frac{D_{10}^2e^3}{1+e}\right)^{0{\cdot}73} \quad (24)$$
$$r = 0{\cdot}95,\ R^2 = 0{\cdot}91,\ n = 30,\ p < 0{\cdot}0001$$

The exponent in equation (24) (0·73) is close to equation (7) (0·78). With R^2 equals to 0·91, the model seems to give good prediction of k in crushed material used in this study. The predicted plotted against measured plot (Fig. 9(b)) shows that nine out of 30 data points lie outside the ±50% margins, within which six out of nine of these data points represent under-predictions; 53·3% of the data points lie above the line of equality and the remainder data of points fall beneath. Therefore, equation (24) gives a slight under-prediction of $k_{20°C}$ for the database.

Grading entropy model

Figure 10 shows the non-dimensional grading entropy coordinates A, B plotted against the measured $k_{20°C}$, D_{10}, C_Z and C_U and indicates that, for unbounded granular mixtures, the variation in coefficient of permeability correlates with A and B. A is positively correlated with permeability, whereas B shows a negative correlation. D_{10} is also positively correlated with $k_{20°C}$. Interesting patterns also emerge from the variation of C_Z and C_U with the non-dimensional grading entropy parameters (Figs 10(e)–10(h)): both high- and

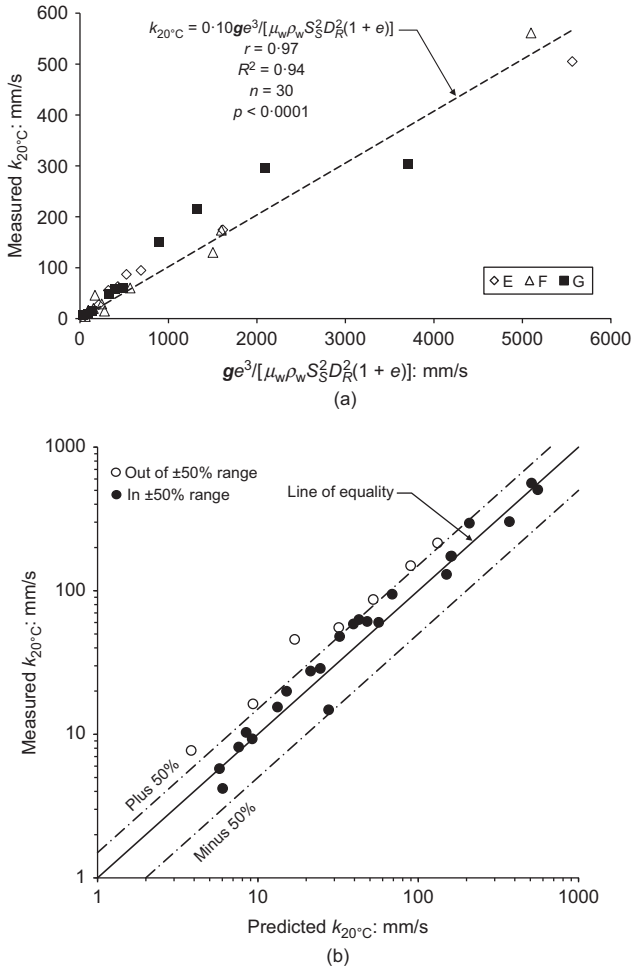

Fig. 8. (a) k plotted against Kozeny–Carman function. (b) Predicted k compared to measured k (equation (22))

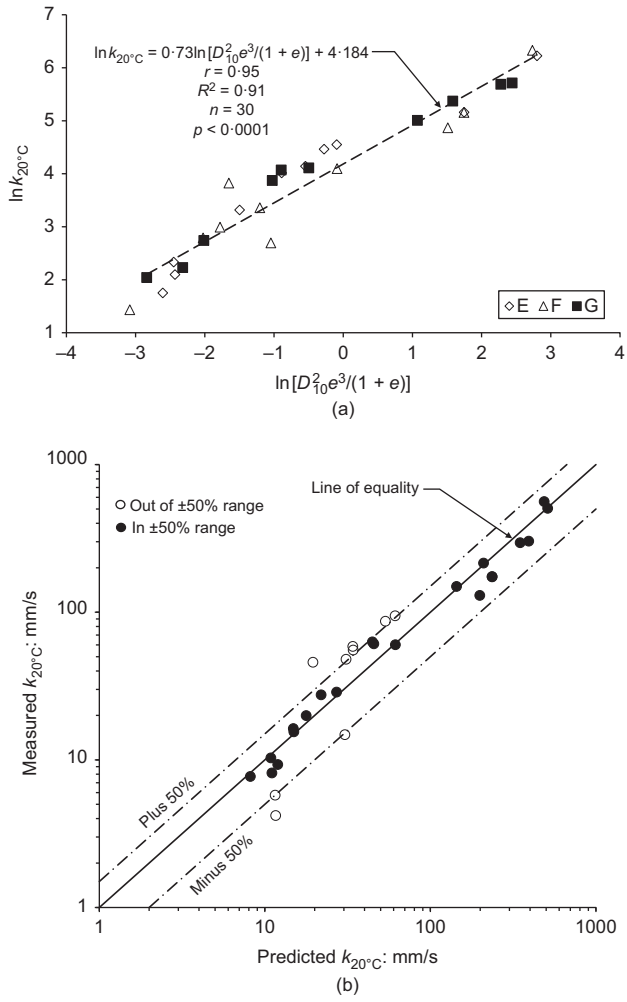

Fig. 9. (a) $\ln k$ plotted against $\ln[D_{10}^2e^3/(1+e)]$. (b) Predicted k compared to measured k (equation (24))

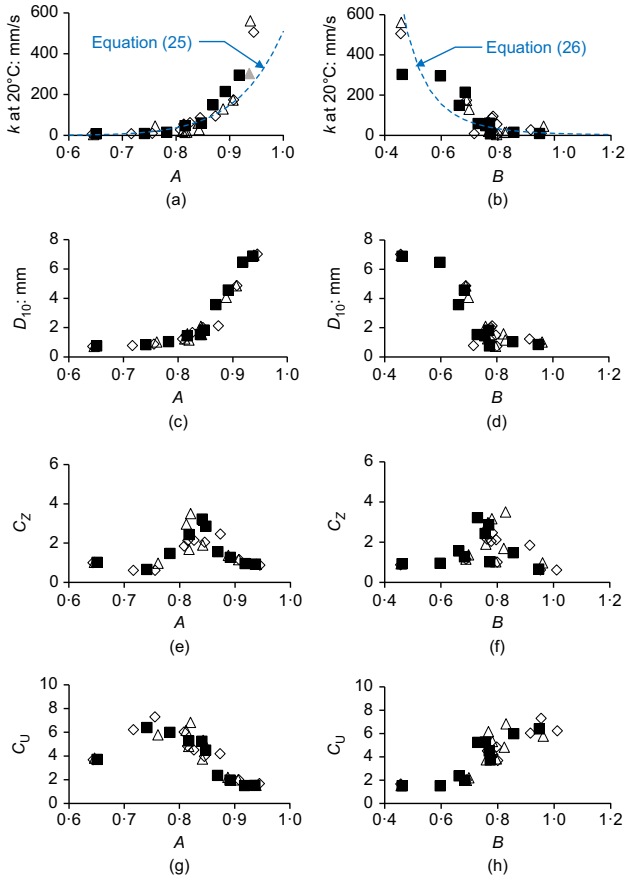

Fig. 10. Normalised entropy plotted against permeability and other parameters (the symbols follow the same usage as in Fig. 6(a))

low-permeability mixtures have constant C_Z values around 1; higher C_Z values that peak around $A = 0{\cdot}82$ and $B = 0{\cdot}78$ are observed; C_U is negatively correlated to A and positively correlated to B. Gradations of tested samples were plotted on the normalised entropy diagram with their corresponding measured permeability categorised into three classes – low k ($k < 10$ mm/s), medium k ($10 < k < 100$ mm/s) and high k ($k > 100$ mm/s) (see Fig. 11); this may be used as a design chart for engineers to make a priori assessments of the tendency of granular mixtures to exhibit high or low permeability.

The regressed results of $k_{20°C}$ with A and B, respectively (Figs 10(a) and 10(b)), are

$$k_{20°C} = 509{\cdot}13A^{11{\cdot}78}$$
$$r = 0{\cdot}91,\ R^2 = 0{\cdot}83,\ n = 30,\ p < 0{\cdot}0001 \quad (25)$$

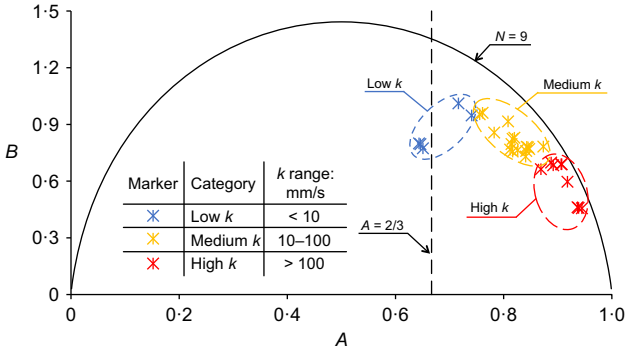

Fig. 11. Identified permeability zones shown on the normalised entropy diagram

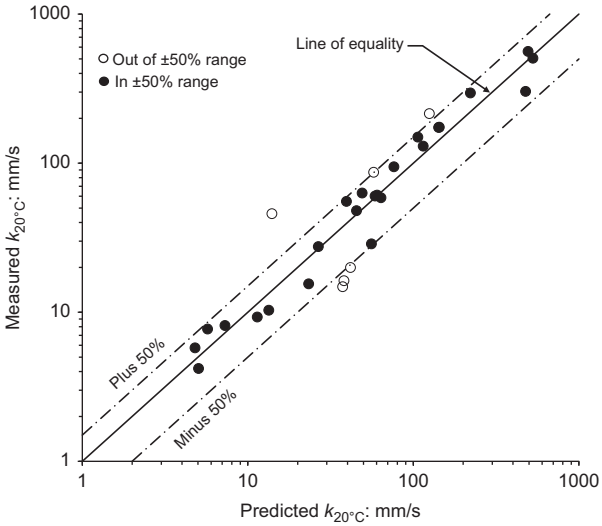

Fig. 12. Predicted k compared to measured k (equation (27))

$$k_{20°C} = 9{\cdot}92B^{-5{\cdot}38}$$
$$r = 0{\cdot}79,\ R^2 = 0{\cdot}63,\ n = 30,\ p < 0{\cdot}0001 \quad (26)$$

Based on the individual regression results, the relative base entropy A ($R^2 = 0{\cdot}83$) which indicates the skewness (symmetry) of a gradation appears to be more closely correlated to $k_{20°C}$ than the normalised entropy increments B ($R^2 = 0{\cdot}63$), which measures the peakiness (kurtosis) of a gradation. The multiple linear regression of $k_{20°C}$ with both A and B included produced the following equation

$$k_{20°C} = 145{\cdot}47A^{8{\cdot}90}B^{-2{\cdot}30}$$
$$r = 0{\cdot}95,\ R^2 = 0{\cdot}90,\ n = 30,\ p < 0{\cdot}0001 \quad (27)$$

The predicted against measured values plot (Fig. 12), shows that six out of 30 data points lie outside the ±50% margins and 46·7% of the data points fall beneath the line of equality, while the remainder of the data points lie above it. This result is a slight under-prediction compared with that obtained with equation (21), but the accuracy is greater in terms of number of values within ±50%. Overall the six points lying outside the ±50% bounds are evenly distributed above and below the line of equality. Equation (22) gives a more reliable prediction of $k_{20°C}$ than equation (27) in terms of R^2; however, it is noted that equation (27) (grading entropy method) does not require that the engineer should measure the void ratio, only the gradation is needed, whereas equation (22) (Kozeny–Carman model) requires both. The normalised grading entropy does not take account of the shape factor of the mixed particles (nor do the three other methods). However, the Kozeny–Carman model does have an empirical shape factor, which according to Garcia *et al.* (2009) is a 'small but noticeable' factor affecting soil permeability, therefore, the coefficient of equation (27) may be a function of particle shape.

SUMMARY

The five models: 'Hazen', 'Shepherd', 'Kozeny–Carman', 'Chapuis' and 'grading entropy' all appear to be statistically reliable in estimating the coefficient of permeability generally to within about ±50%. However, the grading entropy approach (which does not require measurement of void ratio) has produced a predicted against measured values plot that is both essentially evenly distributed about the line of equality and has

only six out of 30 points out of the ±50% prediction bounds. Equation (22) (Kozeny–Carman) yielded the highest R^2 value but the predicted against measured values plot is slightly less symmetrical than that given using equation (27). Examination of the statistical measures (e.g. R^2, p-value) calculated for each model reveals that there is effectively no statistical reason to favour one model over another. However, when examining the results using predicted against measured values plots, both the Kozeny–Carman and grading entropy approaches produce the most accurate results, with Kozeny–Carman being favoured when considering average scatter (R^2) (based on the chosen variant of equation) and grading entropy when considering the number of points within ±50%. However, the coefficients and correlations calculated in equations (18)–(27) only hold for the specific soil tested in this research; testing using mixtures with more diverse gradings and shape factors than those presented here is still needed to further validate the trends shown.

ACKNOWLEDGEMENT

The authors thank Mr Gary Martin for his technical services and support during the testing. Readers may download the online supplementary file from the ICE Virtual Library website.

NOTATION

A	relative base entropy
B	normalised entropy increment
C_H	Hazen empirical coefficient (length^{-1}/time)
C_i	number of elementary cells in a fraction i
$C_{K\text{-}C}$	Kozeny–Carman coefficient
C_U	coefficient of uniformity, $C_U = D_{60}/D_{10}$
C_Z	coefficient of curvature, $C_Z = D_{30}^2/D_{60}D_{10}$
c	dimensionless constant
D_R	specific gravity of solid
D_{10}	effective particle size, for which 10% of the soil is finer (length)
D_{50}	effective particle size, for which 50% of the soil is finer (length)
d_i	width of the fraction i (length)
d_o	width of the elementary cell (length)
e	void ratio
$\boldsymbol{g}$	gravitational acceleration (length/time^2)
K	intrinsic permeability (length^2)
k	coefficient of permeability (length/time)
$k_{20°C}$	coefficient of permeability corrected to 20°C (length/time)
L	length
M	total weight of the sample mixture
M_i	weight of particles in fraction i
m	dry mass of the sample
n	number of data points in a regression
$P_{No\ D} - P_{No\ d}$	percentage by weight of particles between size D (the larger one) and size d (the smaller one)
p	p-value
R^2	coefficient of determination
r	correlation coefficient
S	grading entropy
S_A	specific surface area per unit volume of particles (length^{-1})
S_0	base entropy
S_s	specific surface of the solid
T	time
t	temperature (°C)
V	total volume of the sample
x	exponent
x_i	relative frequency of fraction i
γ	unit weight (force/length^3)
ΔS	entropy increment
μ	dynamic viscosity ((mass/time)/length)
ν	kinematic viscosity (length^2/time)
ρ	density (mass/length^3)

REFERENCES

ASTM (2014). C136/ C136M-14: Standard test method for sieve analysis of fine and coarse aggregates. West Conshohocken, PA, USA: ASTM International.

BSI (1990). BS 1377-Part 5:1990: Determination of permeability by the constant-head method. London, UK: BSI.

Carman, P. C. (1937). Fluid flow through granular beds. *Trans. – Instn Chem. Engrs* **15**, 150–166.

Carman, P. C. (1939). Permeability of saturated sands, soils and clays. *J. Agric. Sci.* **29**, No. 2, 262–273, https://doi.org/10.1017/S0021859600051789.

Carrier, W. D. III (2003). Goodbye, Hazen; hello, Kozeny–Carman. *J. Geotech. Geoenviron. Engng* **129**, No. 11, 1054–1056, https://doi.org/10.1061/(ASCE)1090-0241(2003)129:11(1054).

Chapuis, R. P. (2004). Predicting the saturated hydraulic conductivity of sand and gravel using effective diameter and void ratio. *Can. Geotech. J.* **41**, No. 5, 787–795, https://doi.org/10.1139/t04-022.

Chapuis, R. P. (2012). Predicting the saturated hydraulic conductivity of soils: a review. *Bull. Engng Geol. Built Environ.* **71**, No. 3, 401–434, https://doi.org/10.1007/s10064-012-0418-7.

Chapuis, R. P. & Aubertin, M. (2003). On the use of the Kozeny Carman equation to predict the hydraulic conductivity of soils. *Can. Geotech. J.* **40**, No. 3, 616–628, https://doi.org/10.1139/t03-013.

Chapuis, R. P. & Légaré, P. P. (1992). A simple method for determining the surface area of fine aggregates and fillers in bituminous mixtures. In *Effects of aggregates and mineral fillers on asphalt mixture performance* (ed. R. C. Meininger), STP 1147, pp. 177–186. West Conshohocken, PA, USA: American Society for Testing and Materials (ASTM).

Feng, S. (2017). *Assessing the permeability of pavement construction materials by using grading entropy theory.* MSc thesis, University of Bristol, Bristol, UK.

Feng, S., Vardanega, P. J., Ibraim, E., Widyatmoko, I. & Ojum, C. (2018). Assessing the hydraulic conductivity of road paving materials using representative pore size and grading entropy. *ce/papers* **2**, No. 2–3, 871–876, https://doi.org/10.1002/cepa.780.

Garcia, X., Akanji, L. T., Blunt, M. J., Matthai, S. K. & Latham, J. P. (2009). Numerical study of the effect of particle shape and polydispersity on permeability. *Phys. Rev. E* **80**, No. 2, 021304, https://doi.org/10.1103/PhysRevE.80.021304.

Hazen, A. (1893). *Some physical properties of sand and gravels*, 24th Annual Report. Boston, MA, USA: Massachusetts State Board of Health, Wright & Potter Printing.

Hazen, A. (1895). *The filtration of public water-supplies.* New York, NY, USA: John Wiley & Sons.

Hazen, A. (1911). Discussion of 'Dam on Sand Foundation' by A. C. Koenig. *Trans. Am. Soc. Civ. Engrs* **73**, 199–203.

Holtz, R. D., Kovacs, W. D. & Sheahan, T. C. (2011). *An introduction to geotechnical engineering*, 2nd edn. London, UK: Pearson.

Imre, E. & Fityus, S. (2018). The use of the grading entropy as a measure of the soil text maturity. *ce/papers* **2**, No. 2–3, 639–644, https://doi.org/10.1002/cepa.742.

Imre, E., Lörincz, J. & Rózsa, P. (2008). Characterization of some sand mixtures. *Proceedings of the 12th international conference of international association for computer methods and advances in geomechanics (IACMAG)* (ed. M. N. Jadhav), vol. 3, pp. 2064–2075. Red Hook, NY, USA: Curran Associates.

Imre, E., Lörincz, J., Trang, Q. P., Fityus, S., Pusztai, J., Telekes, G. & Schanz, T. (2009). A general dry density law for sands. *KSCE J. Civ. Engng* **13**, No. 4, 257–272, https://doi.org/10.1007/s12205-009-0257-7.

Imre, E., Lörincz, J., Szendefy, J., Trang, P., Nagy, L., Singh, V. & Fityus, S. (2012). Case studies and benchmark examples for the use of grading entropy in geotechnics. *Entropy* **14**, No. 12, 1079–1102, https://doi.org/10.3390/e14061079.

Imre, E., Nagy, L., Lőrincz, J., Rahemi, N., Schanz, T., Singh, V. P. & Fityus, S. (2015). Some comments on the entropy-based criteria for piping. *Entropy* **17**, No. 4, 2281–2303, https://doi.org/10.3390/e17042281.

James, M. A. (2015). *The grading entropy and permeability of road surfaces*, Undergraduate Project Report. Bristol, UK: University of Bristol.

Kozeny, J. (1927). Über kapillare Leitung des Wassers im Boden (Aufstieg, Versickerung und Anwendung auf die Bewässerung). *Sitzungsber. Akad. Wiss. Wien.* **136a**, 271–306 (in German).

Li, J. & Gu, Y. (2005). Coalescence of oil in water emulsions in fibrous and granular beds. *Separation Purification Technol.* **42**, No. 1, 1–13, https://doi.org/10.1016/j.seppur.2004.05.006.

Lőrincz, J. (1990). Relationship between grading entropy and dry bulk density of granular soils. *Periodica Polytechnica. Civ. Engng* **34**, No. 3, 255–265.

Lőrincz, J., Imre, E., Gálos, M., Trang, Q. P., Rajkai, K., Fityus, S. & Telekes, G. (2005). Grading entropy variation due to soil crushing. *Int. J. Geomech.* **5**, No. 4, 311–319, https://doi.org/10.1061/(ASCE)1532-3641(2005)5:4(311).

Lőrincz, J., Imre, E., Trang, Q. P., Pusztai, J., Telekes, G., Rajkai, K. & Schanz, T. (2008). A general density law for sands. *Proceedings of the 12th international conference of the International Association for Computer Methods and Advances in Geomechanics (IACMAG)* (ed. M. N. Jadhav), vol. 3, pp. 2003–2011. Red Hook, USA: Curran Associates.

Lőrincz, J., Imre, E., Fityus, S., Trang, P. Q., Tarnai, T., Talata, I. & Singh, V. P. (2015a). The grading entropy-based criteria for structural stability of granular materials and filters. *Entropy* **17**, No. 5, 2781–2811, https://doi.org/10.3390/e17052781.

Lőrincz, J., Imre, E., Trang, P. Q., Telekes, G., Nagy, L., Gálos, M., Török, A. & Fityus, S. (2015b). Grading entropy and degradation of sands and rocks. In *Proceedings of the 2nd international electronic conference on entropy and its applications*. Basel, Switzerland: Multidisciplinary Digital Publishing Institute.

Mathavan, G. N. & Viraraghavan, T. (1992). Coalescence/filtration of an oil-in-water emulsion in a peat bed. *Water Res.* **26**, No. 1, 91–98, https://doi.org/10.1016/0043-1354(92)90116-L.

McDougall, J., Kelly, D. & Barreto, D. (2013a). Particle loss and volume change on dissolution: experimental results and analysis of particle size and amount effects. *Acta Geotechnica* **8**, No. 6, 619–627, https://doi.org/10.1007/s11440-013-0212-0.

McDougall, J. R., Imre, E., Barreto, D. & Kelly, D. (2013b). Volumetric consequences of particle loss by grading entropy. *Géotechnique* **63**, No. 3, 262–266, https://doi.org/10.1680/geot.SIP13.T.002.

Ozgumus, T., Mobedi, M. & Ozkol, U. (2014). Determination of Kozeny constant based on porosity and pore to throat size ratio in porous medium with rectangular rods. *Engng Applic. Comput. Fluid Mech.* **8**, No. 2, 308–318, https://doi.org/10.1080/19942060.2014.11015516.

Shannon, C. E. (1948). A mathematical theory of communication. *Bell System Tech. J.* **27**, No. 3, 379–423, https://doi.org/10.1002/j.1538-7305.1948.tb01338.x.

Shepherd, R. G. (1989). Correlations of permeability and grain size. *Ground Water* **27**, No. 5, 633–638, https://doi.org/10.1111/j.1745-6584.1989.tb00476.x.

Singh, V. P. (2014). *Entropy theory in hydraulic engineering: an introduction*. Reston, VA, USA: American Society of Civil Engineers.

Thom, N. (2014). *Principles of pavement engineering*, 2nd edn. London, UK: Thomas Telford.